IVYSPRING
INTERNATIONAL PUBLISHER

𝕋heranostics

Research Paper

Image-guided chemotherapy with specifically tuned blood brain barrier permeability in glioma margins

Xihui Gao[1, 7, *], Qi Yue[2, *], Yikang Liu[3], Dandan Fan[1], Kun Fan[4], Sihan Li[1], Jun Qian[1], Limei Han[1], Fang Fang[5], Fulin Xu[1], Daoying Geng[6], Liang Chen[2,✉], Xin Zhou[5], Ying Mao[2] and Cong Li[1,6,✉]

1. Minhang Branch, Zhongshan Hospital and Key Laboratory of Smart Drug Delivery, Ministry of Education, School of Pharmacy, Fudan University, Shanghai, China.
2. Department of Neurosurgery, Huashan Hospital, Fudan University, Shanghai, China.
3. Department of Biomedical Engineering, The Pennsylvania State University, University Park, PA, USA
4. Department of Pancreatic and Hepatobiliary Surgery, Fudan University Shanghai Cancer Center, Shanghai, China
5. National Center for Magnetic Resonance in Wuhan, State Key laboratory of Magnetic Resonance and Atomic and Molecular Physics, Wuhan Institute of Physics and Mathematics, Chinese Academy of Sciences, Wuhan, Hubei Province, China
6. Institute of Functional and Molecular Medical Imaging, Department of Radiology, Huashan Hospital, Fudan University, Shanghai, China.
7. Department of Laboratory Medicine, Shanghai Fengxian District Central Hospital, Shanghai, China.

*These authors share equal first authorship.

✉ Corresponding authors: Cong Li, Email: congli@fudan.edu.cn; Liang Chen, Email: hschenliang@fudan.edu.cn

Abstract

Blood–brain barrier (BBB) disruption is frequently observed in the glioma region. However, the tumor uptake of drugs is still too low to meet the threshold of therapeutic purpose.

Method: A tumor vasculature-targeted nanoagonist was developed. Glioma targeting specificity of the nanoagonist was evaluated by *in vivo* optical imaging. BBB permeability at the glioma margin was quantitatively measured by dynamic contrast enhanced magnetic resonance imaging (DCE-MRI). Single-photon emission computed tomography imaging/computed tomography (SPECT/CT) quantitatively determined the glioma uptake of the radiolabeled model drug. T2-weighted MRI monitored the tumor volume.

Results: Immunostaining studies demonstrated that the BBB remained partially intact in the invasive margin of patients' gliomas regardless of their malignancies. DCE-MRI showed that vascular permeability in the glioma margin reached its maximum at 45 min post nanoagonist administration. *In vivo* optical imaging indicated the high glioma targeting specificity of the nanoagonist. SPECT/CT showed the significantly enhanced glioma uptake of the model drug after pre-treatment with the nanoagonist. Image-guided paclitaxel injection after nanoagonist-mediated BBB modulation more efficiently attenuated tumor growth and extended survival than in animal models treated with paclitaxel or temozolomide alone.

Conclusion: Thus, image-guided drug delivery following BBB permeability modulation holds promise to enhance the efficacy of chemotherapeutics to glioma.

Key words: image-guided chemotherapy, dynamic contrast-enhanced magnetic resonance imaging, blood-brain-barrier, glioma margin, nanoagonist

Introduction

Gliomas accounts for approximately 80% of primary malignant brain tumors [1]. Despite aggressive treatment including maximum debulking surgery, radiotherapy and chemotherapy, glioma patients still face dismal prognosis [2]. Among the numerous chemotherapeutics approved for cancer treatment, only a few, such as temozolomide (TMZ), show efficacy towards glioma [3]. In addition to drug resistance, the reason is likely, at least in part, due to their inability to circumvent the blood–brain barrier

(BBB) that maintains brain homeostasis by shielding the brain from peripheral circulation [4, 5]. Despite BBB breakdown in glioma parenchyma, uncompromised BBB is believed to exist in invasive edges of gliomas allowing the cancer cells to infiltrate into surrounding brain tissue [6]. Considering most recurrences occur in the glioma margins [7], strategies specifically delivering therapeutics into the tumor periphery by circumventing the BBB are direly needed.

Up-regulating para-endothelial diffusion is an attractive strategy to increase the brain delivery of drugs by maximally preserving their pharmacological potencies. Hypertonic agents such as mannitol have been used in the clinic to break para-endothelial tight junctions (TJs) via osmotic pressure [8]. However, non-selective BBB disruption results in complications such as epileptic seizures and brain edema [9]. Microbubble-enhanced focused ultrasound (MB-FUS) was also used to facilitate brain drug delivery by disrupting TJs via bubble oscillation-induced microstreaming forces [10]. Nevertheless, mechanical shear force-induced potential risks, including cerebral hemorrhage and excessive immune reaction, cannot be overlooked [11]. Therefore, up-regulating vascular permeability in glioma marginal territories with high efficiency, specificity and safety is highly desirable.

Adenosine 2A receptor ($A_{2A}R$) is a purinergic G-protein coupled receptor (GPCR) with adenosine as an endogenous agonist. Signaling vascular $A_{2A}R$ with its agonist could increase BBB permeability by temporarily opening TJs [12]. We previously developed a series of $A_{2A}R$ nanoagonists that not only more efficiently modulated BBB permeability than small molecule agonists, but also showed capability of tuning the BBB opening time window [13, 14]. Importantly, minimal side effects were observed even after multiple cycles of BBB modulation [15, 16]. In this study, we developed a new nanoagonist in which glioma-targeting ligands and $A_{2A}R$ agonistic domains were modified on a nanoplatform. We hypothesized that this nanoagonist would first target the glioma neovasculature and then compromise peri-tumoral BBB integrity via $A_{2A}R$ signaling. The chemotherapeutic is injected when the BBB permeability is imaged to be high in the glioma margin but low in the surrounding brain tissue. Therefore, the efficiency of chemotherapeutics could be maximized by specifically increasing BBB permeability in the tumor invasive margin. The aim of this study is to up-regulate chemotherapeutic efficiency by specifically increasing blood brain barrier permeability in the glioma invasive margin.

Results

Tight junction-associated protein ZO-1 remains partially intact in patient glioma margins

Although uncompromised BBB in the glioma margin is believed to be the primary cause of the low chemotherapeutic efficiency [17], there is insufficient clinical evidence to support this notion. To address this issue, ZO-1, a key TJ-associated protein that determines BBB integrity, was immuno-stained in the marginal regions of low-grade glioma (LGG) and high-grade glioma (HGG) from patients, as well as in control brain tissues (**Figure 1A**). While ZO-1 immunity was presented as well-regulated zebra-strips twining around vascular endothelium in control brain tissues, its disrupted distribution and attenuated expression level in glioma margins were evident. Nevertheless, capillaries with unspoiled ZO-1 immunity were still present in the marginal territories regardless of the malignancy grade. The capillary percentage with intact ZO-1 was decreased from 74.1% in control brain tissues to 48.5% in LGG and 23.7% in HGG (**Figure 1B**). The highest ZO-1 expression level was found in control brain tissues, which was 1.45- and 3.17-fold higher than that in LGG and HGG respectively (**Figure 1C**). Representative *he*matoxylin-eosin (H&E)-stained images of LGG, HGG and control brain tissue sections are presented in **Figure S1**. Neurons, glial cells and vascular endothelial cells distributed dispersedly and were well-organized in control human brain tissues. In the LGG margin, the cells distributed with a slightly higher density than in the control brain tissues and mild shape abnormality was observed. Also, neuronophagia and blurred structures were observed. In the HGG margin, the cell density was substantially higher than that of the control brain and LGG margin. Remarkable shape abnormality and karyokinesis with higher nucleus to cytoplasm ratio were observed. Additionally, the normal structure of brain tissue disappeared and disorderedly distributed vasculature and necrosis were evident.

Over-expression of both $A_{2A}R$ and β_3 integrin in patient glioma margins

The presence of both $A_{2A}R$ and $\alpha_v\beta_3$ integrin in the glioma margin is a prerequisite to specifically tune BBB permeability in the glioma margin. As expected, no obvious β_3 integrin was detected in the vessels of control brain tissues (**Figure 2A**). By contrast, pronounced β_3 integrin immunity polarized on the luminal face of the vasculature in HGG margins was demonstrated. While vascular $A_{2A}R$ immunity remained faint in control brain tissue, it increased
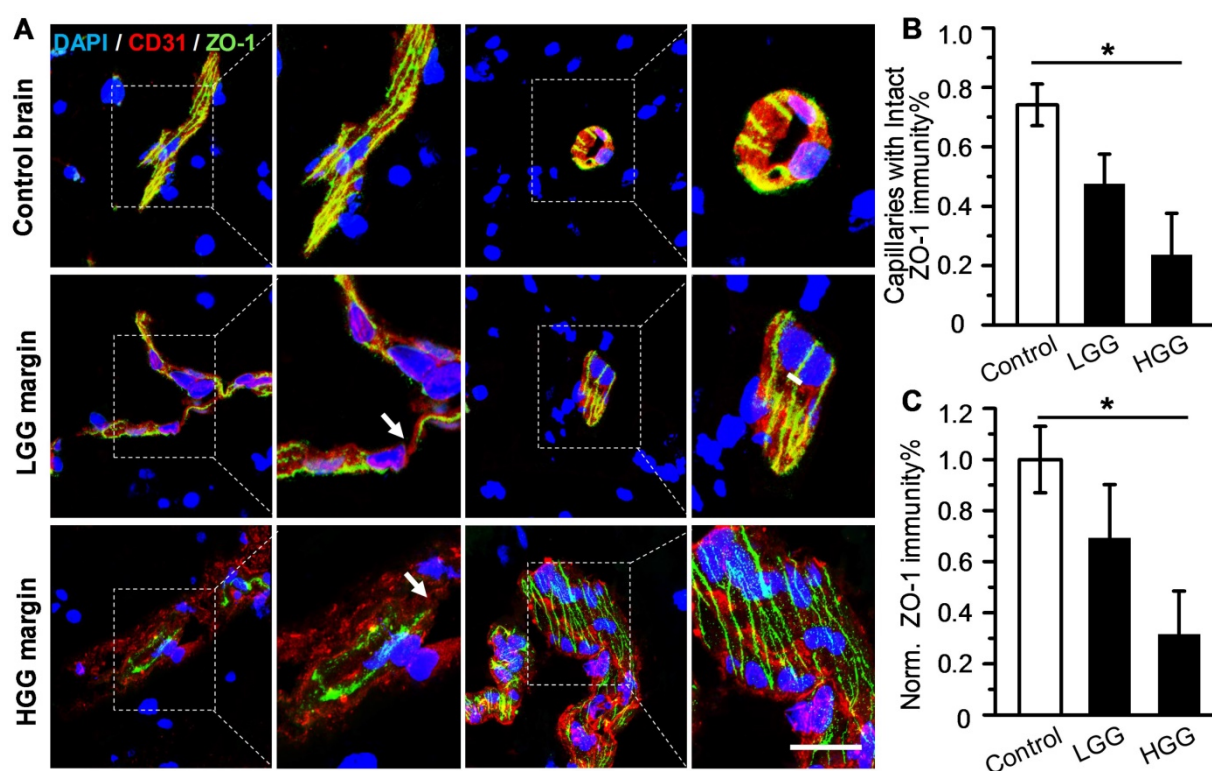
Figure 1. Uncompromised TJ associated protein is found in the glioma margin from patients. (A) Representative immunofluorescence images of vascular endothelium and ZO-1 protein in control brain tissues and invasive margins of LGG and HGG. Endothelium stained by CD31 antibody is displayed in red, ZO-1 immunity is displayed in green; the nucleus stained with DAPI is shown in blue. Scale bar: 30 μm. **(B)** Percentage of capillaries with intact ZO-1 immunity in control brain tissues and glioma margins (control brain tissue, n = 4, LGG, n = 3, HGG, n = 5). *$P \leq 0.05$ control brain tissue vs HGG. **(C)** Normalized vascular ZO-1 immunities in control brain and glioma margins. *$P \leq 0.05$ control brain tissue vs. HGG. LGG: low-grade glioma; HGG: high-grade glioma; TJ: tight junction.

remarkably in the tumor margins (**Figure 2B**). Compared to the control brain tissue, $A_{2A}R$ and β_3 integrin immunities were increased by 53% and 69.4%, respectively, in LGG and 57% and 213.5%, respectively, in HGG (**Figure 2C**).

Nanoagonist compromises TJs in the brain endothelial monolayer

In this work, a new nanoagonist Den-RGD-Reg was developed that was expected to first target the glioma neovasculature and then compromise peri-tumoral BBB integrity via $A_{2A}R$ signaling. The small molecule $A_{2A}R$ agonist regadenoson, nanoparticle Den-Reg without a tumor targeting group, and Den-PEG without any functional group were selected as control groups. The chemical structures of the small molecule agonist regadenoson, nanoagonist Den-RGD-Reg, control nanoparticle Den-Reg, and Den-PEG are presented in **Figure 3A**. Detailed synthetic procedures are presented in **Figure S2**. The agonistic domain Reg-NH$_2$ and c(RGDyK) peptide were labeled on the fifth generation (G5) poly(amidoamine) (PAMAM) dendrimer through poly(ethylene glycol) (PEG) linkers. The home-made, near-infrared (NIR) fluorophore IR640B was directly modified on the dendrimer surface. ^{1}HNMR of Den-RGD-Reg indicated that the molar ratio between

the c[RGDyK] peptide/agonist domain/dendrimer was 8.2/11.4/23.3/1 (see Supplementary Material). TEM images showed the nanoagonist to be well-separated spherical particles with diameters in the range of 6–8 nm (**Figure S3A**). The hydrodynamic diameter of the nanoagonist was measured as 7.9 nm, while its surface charge was measured as +16.5 mV (**Figure S3B**).

ZO-1 is a TJ-associated protein that links cell adhesion molecules to actin cytoskeleton for maintaining morphology of endothelial cells. While ZO-1 protein was expressed as a continuous alignment on the cell-cell interface of intact BBB, the discontinued intervals and even absence this protein can be observed in compromised BBB. Mouse brain capillary endothelial bEnd.3 cells were cultured to reach 100% confluence. After treatment with PBS, 10 μM regadenoson, or nanoagonist, the cells were immunostained with anti-ZO-1 antibody. As shown in **Figure 3B**, ZO-1 immunity as continuous and sharp lines delineated the para-cellular interface of cultured mouse brain capillary endothelial bEnd.3 cells. Although treatment with both regadenoson and the nanoagonist led to ZO-1 disruption, nanoagonist treatment led to more significant ZO-1 breakdown than regadenoson treatment. Actin stress fibres

(ASFs) were also stained after the bEnd.3 cells were treated with PBS, 10 μM regadenoson, or nanoagonist. Results showed that $A_{2A}R$ signaling triggered the formation of ASFs, leading to cell contraction followed by TJ disassembly. While ASFs were distributed as short, thin fibers aligned to the longitudinal axis of the endothelial cells, their length and thickness increased dramatically after agonist addition. Nanoagonists induced ASF assembly more efficiently than regadenoson. After treatment with regadenoson or the nanoagonist, the ZO-1 immunofluorescence intensity levels were decreased by 17% and 48%, respectively, with the simultaneous increase in average ASF fluorescence intensity levels by 1.9- and 2.9-fold, respectively (**Figure 3C**). Immunoblotting studies revealed the attenuation of TJ-associated proteins ZO-1 (16%) and occludin (7%) at 30 min after agonist addition (**Figure 3D**). Cytoskeletal rearrangement promotes conversion of G-actin to F-actin, a sign of ASF formation. The F/G-actin ratio in bEnd.3 cells was determined to be 1.32 after nanoagonist treatment, which was significantly higher than that of regadenoson (0.98) or PBS (0.92). Phosphorylation of myosin light chain (MLC) protein triggers the formation of ASF from short F-actins to elicit cytoskeletal contraction. As expected, while the total MLC level was unchanged after agonist addition, phosphorylated MLC (pMLC) increased significantly. The pMLC/MLC ratios at 30 min post treatment of nanoagonist or regadenoson were measured to be 1.02 and 0.97, respectively, both significantly higher than that (0.53) following PBS treatment.

Nanoagonist specifically tunes BBB permeability in the glioma margins

In vivo NIR fluorescence images demonstrated that the nanoagonist offered a higher target to background (T/B) ratio (1.83 ± 0.84) than Den-Reg (1.21 ± 0.43) or Den-PEG (1.10 ± 0.27) at 24 h post i.v. injection (39.3 mg/mouse) in mice bearing orthotopic U87MG glioma xenografts (**Figure S4**). The T/B of the nanoagonist in excised mouse brain tissue was 2.32 ± 0.76, which was significantly higher than that of Den-Reg (1.46 ± 0.51) or Den-PEG (1.26 ± 0.38). Fluorescence microscopy imaging showed that, while a strong fluorescence signal of nanoagonist occupied the entire tumor region, only scattered intratumoral signals of Den-Reg or Den-PEG were observed (**Figure S5**).
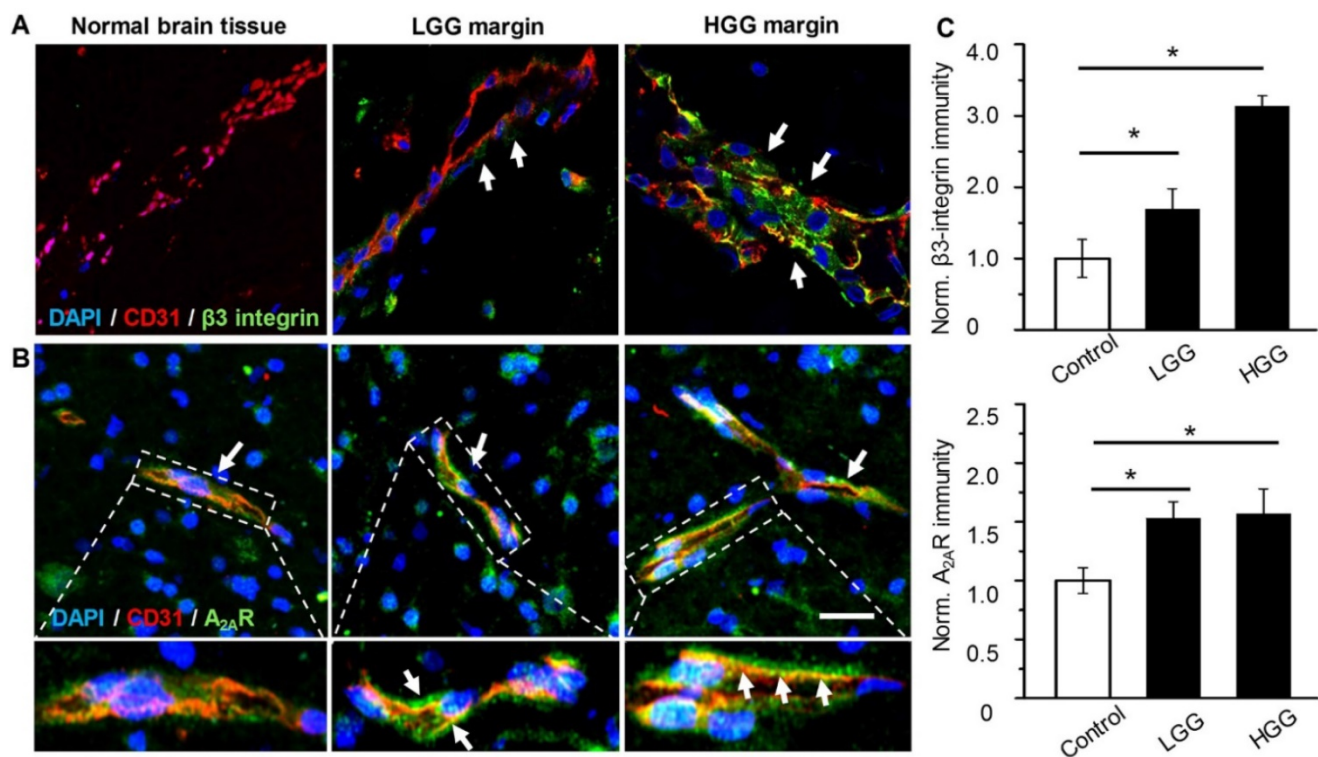

Figure 2. Over-expressed vascular A₂ₐR and β3 integrin in glioma margins from patients. Representative immunofluorescence images for vascular endothelium and β3 integrin **(A)** or A₂ₐR **(B)** in control brain tissue and glioma margins. Endothelial immunity is displayed in red, A₂ₐR or β3 immunity is displayed in green. Scale bar: 50 μm. Perivascular A₂ₐR or β3 immunity is indicated by the arrows. **(C)** Normalized immunofluorescent intensities of perivascular A₂ₐR or β3 in control brain tissue and glioma margins (brain tissue, n = 4; LGG, n = 3; HGG, n = 5). *P ≤ 0.05 control tissue vs. LGG or HGG. ***P ≤ 0.001 control tissue vs HGG.
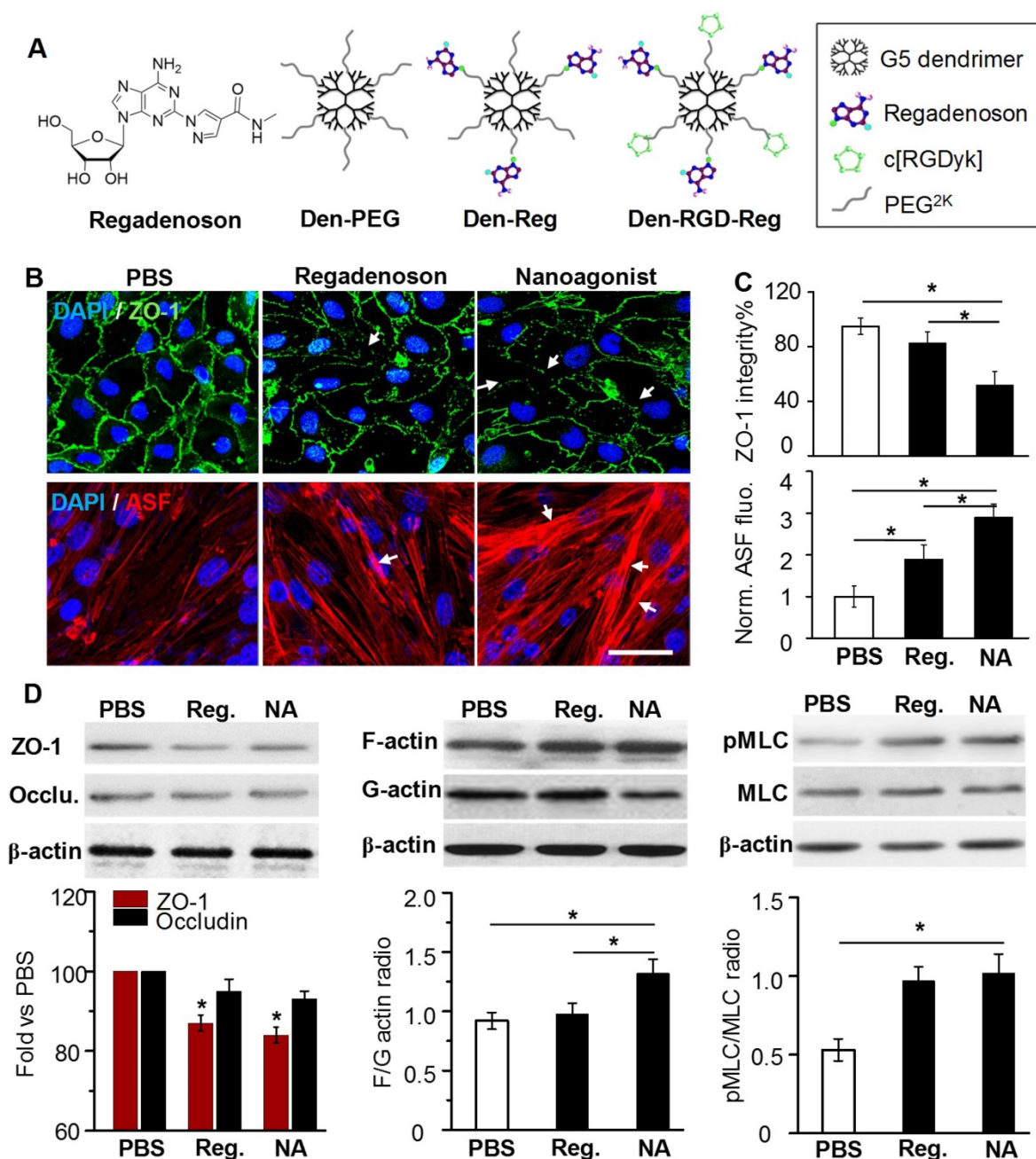
Figure 3. Nanoagonist attenuates para-endothelial TJs in the endothelial monolayer. (A) Chemical structures of regadenoson, nanoagonist Den-RGD-Reg, control nanoparticles Den-Reg and Den-PEG. **(B)** Fluorescence microscopic images of ZO-1 and ASF in the bEnd.3 endothelial monolayer at 30 min post treatment. Arrows point to disrupted ZO-1 (upper panel) and newly formed ASF (lower panel). Scale bar: 50 μm. **(C)** Percentage of ZO-1 integrity and normalized ASF fluorescence intensity at 30 min post treatment of PBS, regadenoson or nanoagonist (n = 4). *$P \leq 0.05$ nanoagonist versus PBS and regadenoson, regadenoson versus PBS. **(D)** The nanoagonist triggered MLC phosphorylation, actin aggregation and attenuation of TJ-associated proteins. β-actin was used as an internal loading control. *$P \leq 0.05$, nanoagonist vs. PBS and regadenoson, regadenoson vs. PBS. TJ: tight junction; ASF: actinomyosin stress fibre; Reg: regadenoson; MLC: myosin light chain protein; NA: nanoagonist.

In vivo T2W MRI visualized the glioma xenografts with a hyper-intense signal (**Figure 4A**). The tumor could not be distinguished well by T1W-MRI until the injection of Gd^{3+}-DTPA. Interestingly, compared with the glioma xenograft defined by Gd^{3+}-DTPA alone, the tumor margin was extended substantially when Gd^{3+}-DTPA was injected post nanoagonist administration. The BBB permeability alteration was quantified by dynamic contrast-enhanced magnetic resonance imaging (DCE-MRI), in which the pixel maps of K_{trans}, a parameter presenting vascular permeability by counting the volume transfer efficiency of a paramagnetic agent between blood and the extracellular extravascular interstitium, are presented. When blood flow is not big enough compared to permeability-surface area product (PS), K_{trans} in the Tofts model is related to both blood flow and PS.
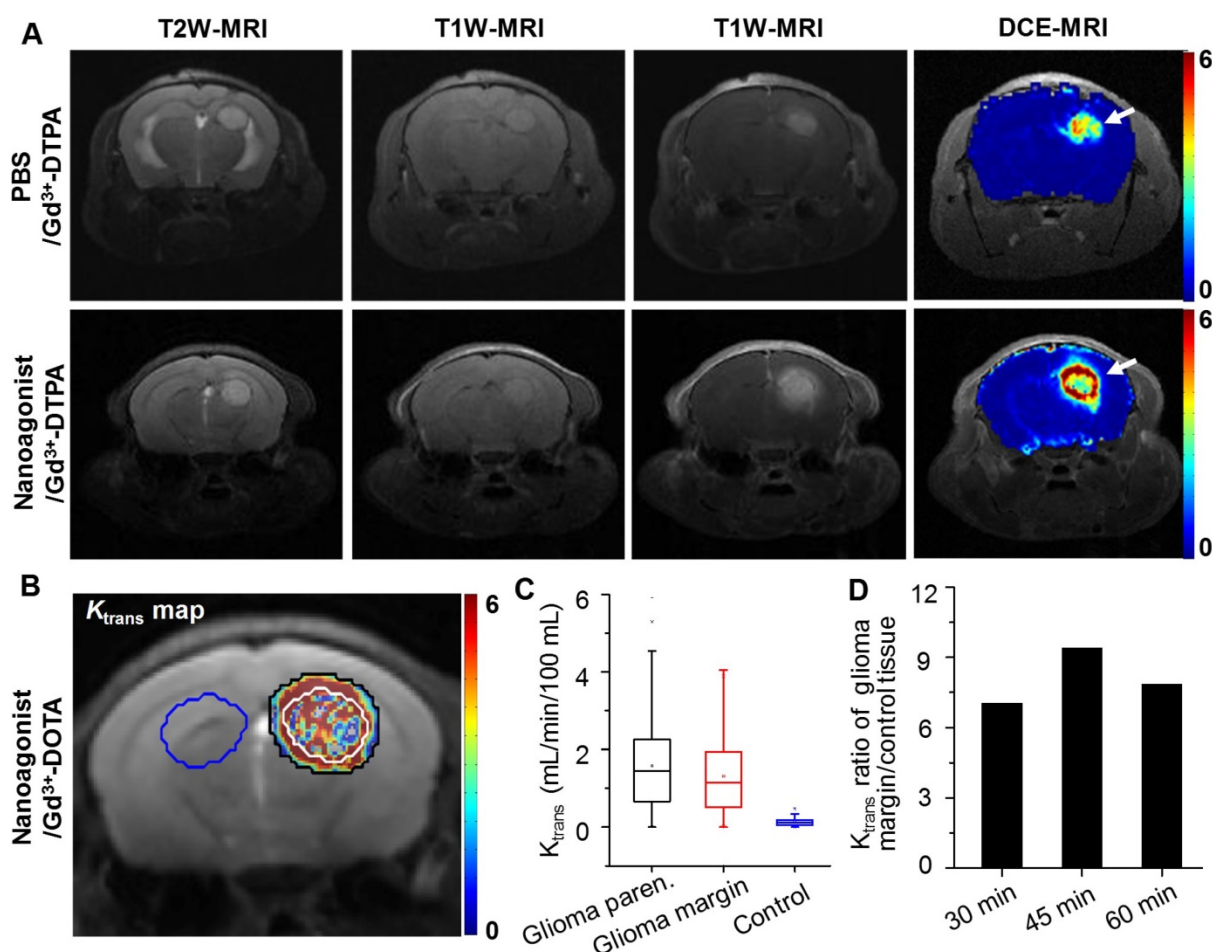
Figure 4. Nanoagonist increases BBB permeability in the margin of glioma xenografts. (A) Representative T2W-, T1W- and DCE-MR images of an identical mouse after treatment with Gd^{3+}-DTPA alone (upper panel) followed by combined treatment of Den-RGD-Reg plus Gd^{3+}-DTPA (lower panel). The combined treatment was conducted at 24 h post the initial Gd^{3+}-DTPA injection. **(B)** K_{trans} maps of mouse brain when Gd^{3+}-DTPA was injected at 45 min post nanoagonist administration. White line circles the tumor parenchyma, tumor margin is delineated between the white and black circles, blue circle selects the control brain tissue. **(C)** Average K_{trans} values in glioma parenchyma, glioma margin and control brain tissue when Gd^{3+}-DTPA was injected at 45 min PI of the nanoagonist (n=3). **(D)** The K_{trans} value ratio between the glioma margin and control brain tissue when Gd^{3+}-DTPA was injected at selected time-points post nanoagonist administration.

However, normal brain tissue is considered to have high blood flow and low permeability due to BBB. In brain tumor imaging, it is often assumed that the leakage is small compared to the high blood supply, which is the reason why the Tofts model is widely used for assessing BBB disruption in tumors. Therefore, in this study, it is reasonable to associate K_{trans} only with BBB permeability.

Compared with the K_{trans} map post treatment with Gd^{3+}-DTPA alone, the combined treatment of nanoagonist followed by Gd^{3+}-DTPA remarkably enhanced the K_{trans} signal in both the glioma parenchyma and margin but not in the normal brain tissue (**Figure 4B**). Importantly, the mean K_{trans} value in the glioma margins increased from 0.05 mL/min/100 mL before nanoagonist treatment to the maximum of 1.2 mL/min/100 mL at 45 min post nanoagonist administration (**Figure 4C** and **Figure S6**). This value decreased to 0.7 mL/min/100 mL at 60 min. The K_{trans} value ratio between the glioma margin

and control brain tissue reached its maximal value (9.5) when Gd^{3+}-DTPA was injected at 45 min post nanoagonist administration (**Figure 4D**). Immunofluorescence study showed remarkable ZO-1 down-regulation in the glioma margins at 30 min post nanoagonist administration (**Figure S7**).

Figure 5A demonstrates SPECT/CT images of the mouse brain area after i.v. injection of ^{99m}Tc-DTPA alone or combined administration of nanoagonist plus ^{99m}Tc-DTPA. According to the DCE-MRI results, ^{99m}Tc-DTPA was injected at 45 min post nanoagonist administration. In contrast to the weak intratumoral radioactivity after the injection of ^{99m}Tc-DTPA, combined treatment offered higher tumor-to-normal brain radioactivity per unit volume ratio (2.96 ± 0.43 vs. 1.17 ± 0.15) (**Figure 5B**). **Figure 5C** shows autoradiographic images of consecutively sectioned mouse brain slides following combined treatment with nanoparticle plus ^{99m}Tc-DTPA. The relative radioactivity in glioma post nanoagonist plus

^{99m}Tc-DTPA treatment was measured as 4.85 ± 0.68, which was 3.2 and 1.9 times higher than that treated with Den-PEG (1.52 ± 0.17) or Den-Reg (2.54 ± 0.39) plus ^{99m}Tc-DTPA (**Figure 5D**).

Image-guided drug administration increases the chemotherapeutic efficiency

Figure 6A presents T2W-MR images of mice bearing U87MG glioma xenografts at selected time points post treatment with Den-RGD-Reg plus PTX, PTX alone, TMZ alone or PBS. In the control group treated with PBS, the average tumor volume increased 11.4 times from 15.6 mm³ at 14 days post tumor implantation to 193.1 mm³ at 28 days (**Figure 6B**). While treatment with PTX alone barely inhibited glioma growth (9.7-fold volume increase at 28 days), a remarkable tumor growth delay (2.9-fold) was observed after the combined treatment of nanoagonist

plus PTX. TMZ showed less therapeutic efficiency than the combined treatment and a 5.4-fold tumor volume increase was recorded. Compared with the PBS-treated mice with a maximal survival time of 29 days after tumor implantation, all of the mice receiving PTX injection succumbed to death at day 32 (**Figure 6C**). Notably, while only 15% of mice after TMZ treatment survived to day 35, and 43% of mice receiving the combination of nanoagonist plus PTX were alive at that time. Terminal-deoxynucleotidyl-transferase mediated dUTP nick end labeling (TUNEL) staining showed that apoptotic cells were predominately located in the tumor but not in normal brain tissue 3 weeks after the combined nanoagonist/PTX administration, implying the safety of this treatment (**Figure S8**).
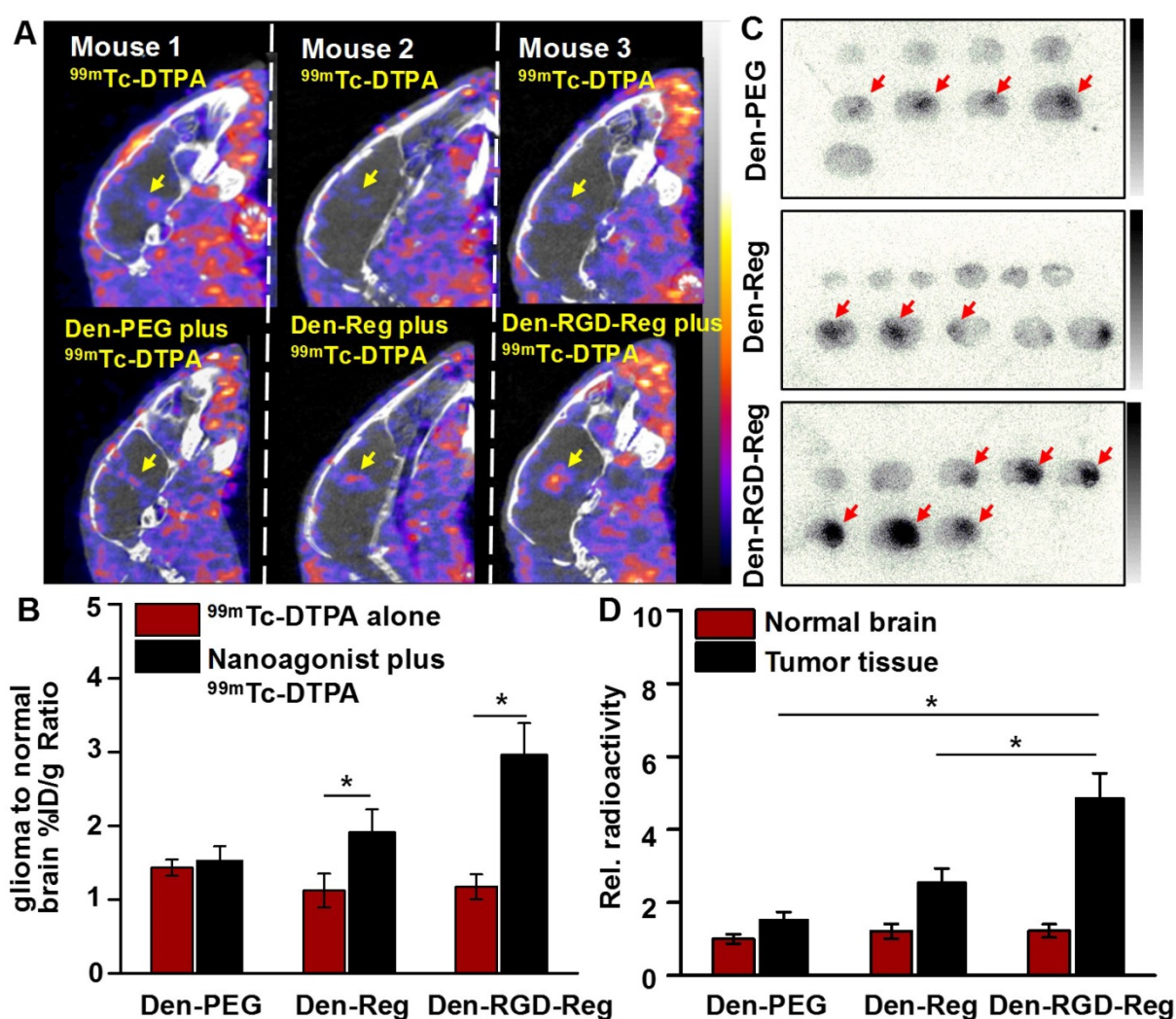

Figure 5. Nanoagonist increases the model drug uptake in glioma xenografts. (A) In vivo SPECT/CT images of the mouse brain area after intravenous injection of ^{99m}Tc-DTPA alone followed by combined treatment of Den-PEG plus ^{99m}Tc-DTPA (mouse 1), Den-Reg plus ^{99m}Tc-DTPA (mouse 2) or Den-RGD-Reg plus ^{99m}Tc-DTPA (mouse 3). The combined treatment was applied at 48 h post initial ^{99m}Tc-DTPA injection. ^{99m}Tc-DTPA as a model drug was injected at 45 min PI of the nanoparticle. **(B)** Glioma to normal brain %ID/g ratio (n = 4) in which ^{99m}Tc-DTPA (3.7×10⁶ Bq/ mouse) was injected at 45 min post administration of PBS, Den-Reg or Den-RGD-Reg. *$P \leq 0.05$ nanoparticle vs. PBS. **(C)** Autoradiographic images of mouse brain sections at 90 min post-injection of ^{99m}Tc-DTPA (n = 4). The arrows indicate glioma. **(D)** Relative radioactivity of ^{99m}Tc-DTPA in the normal brain and glioma areas quantitated from autoradiographic images (n = 4). *$P \leq 0.05$ Den-RGD-Reg vs. Den-PEG. *$P \leq 0.05$ Den-RGD-Reg vs. Den-Reg.
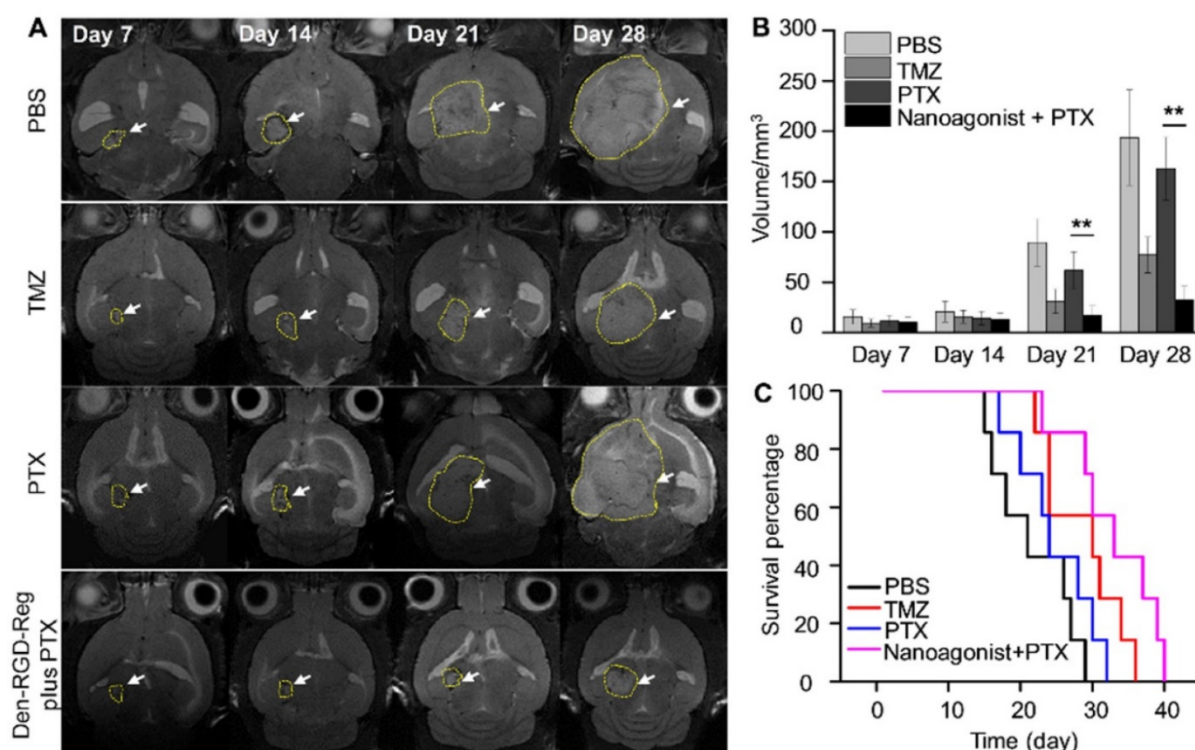
Figure 6. Image-guided drug administration post BBB intervention enhances the chemotherapeutic efficacy. (A) Representative in vivo T2W-MRI of the mouse brain bearing glioma xenograft at selected time-points post treatment of PBS, TMZ (20 mg/kg daily), PTX (5 mg/kg every three days) or nanoagonist (39.3 mg/kg) plus PTX (5.0 mg/kg). The dashed line delineates the tumor margins. Tumor size **(B)** and survival rate **(C)** of the mouse models (n = 7 per group) post corresponding treatment. **P ≤ 0.01 nanoagonist plus PTX versus PTX alone. PTX: Paclitaxel; TMZ: temozolomide.

Discussion

In an *ex vivo* study, TJ breakdown in glioma from patients was evident with a disrupted para-endothelial profile and down-regulated expression level of ZO-1. Glioma cells aggressively invaded neighboring brain tissue by inserting themselves into the perivascular space between the astrocytic endfeet and the endothelium of pre-existing blood vessels, thus disrupting astrocyte-vascular coupling and resulting in a loss of TJ integrity [18]. To the best of our knowledge, this work, for the first time, revealed the unspoiled ZO-1 profile in the marginal region of both HGG and LGG, indicating the existence of uncompromised TJs even in the most malignant glioma. The data highlighted the necessity to deliver chemotherapeutics into glioma margins by overcoming uncompromised TJs.

Current BBB opening strategies can be roughly classified into physical and chemical approaches. Hypertonic chemicals such as mannitol have been used to disrupt the TJs and increase BBB permeability by inducing osmotic pressure between the vascular walls. However, the non-specific BBB breakdown leads to potential risks such as epileptic seizures and vasogenic edema. Focused ultrasound (FUS) has been intensively investigated to locally disrupt BBB [19]. Even though this strategy significantly increased the

therapeutic efficacy of gliomas, the limited focal depth (< 3 cm), the requirement for image-guidance and the thermally induced irreversible BBB recovery need to be overcome. Therefore, specifically and safely tuning BBB permeability is crucial for improving the therapeutic efficiency of gliomas. Compared with hypertonic agents and MB-FUS breaking TJs via external force, the nanoagonist modulates TJ tightness by amplifying the endogenous $A_{2A}R$ signaling cascade. Our previous study showed that the brain uptake of a radioactively labeled dextran (45 kDa) as a macromolecular model drug increased 6.8 times after pretreatment with the nanoagonist [13]. Additionally, the BBB opening time window could be tuned in a range from 30 min to 4 h by adjusting the agonistic domains labeled on the dendrimer. Furthermore, the nanoagonist-modulated BBB permeability reversibly without disrupting the neurovascular units. Pathological symptoms including hemorrhage and edema induced by uncontrollable vascular leakage were not observed after nanoagonist treatment [14]. Thus, nanoagonist-mediated $A_{2A}R$ signaling is a promising strategy to increase brain drug delivery with high efficiency and safety.

Although the precise mechanism of $A_{2A}R$-mediated BBB permeability alteration remains unclear, $A_{2A}R$ activation up-regulates Rho-associated protein kinase (ROCK) activity, which inhibits MLC

phosphatase (MLCP) and thereby promotes the phosphorylation of MLC [20]. MLC phosphorylation promotes the conversion of short F-actins to ASF whose centripetal tension weakens para-endothelial connectivity, disassembles TJ proteins and finally enhances BBB permeability [21]. Both regadenoson and nanoagonist led to an increased F/G-actin ratio and MLC phosphorylation level but reduced TJ-associated protein level in the endothelial monolayer. The above phenomena indicate that both the nanoagonist and small-molecule agonists induced stress fibre formation and TJ opening via $A_{2A}R$ signaling. Notably, the nanoagonist tuned the TJ integrity in a more pronounced manner than the small-molecule agonist. The multivalent association between the nanoagonist and dimeric or even oligomeric $A_{2A}R$ complexes could amplify the receptor-mediated signal transduction and pharmacological responses [22].

The expression levels of both $A_{2A}R$ and β_3 integrin were found to be high in the vasculature of high-grade glioma but low in peritumor control brain tissue, indicating the feasibility to specifically tune BBB permeability in glioma patients. Regadenoson, a purine nucleotide derivative approved by the FDA as a coronary vasodilator, was selected as an agonistic agent due to its high selectivity to $A_{2A}R$ (13-fold against A_1R and > 35-fold against $A_{2B}R$) [23]. The c(RGDyK) peptide was chosen as a targeting ligand to $\alpha v\beta3$ integrin because of its high affinity (1.3 nM) [24]. Considering the stronger association between the c(RGDyK) peptide and $\alpha v\beta3$ integrin than that between regadenoson and $A_{2A}R$ (290 nM), the nanoagonist first targets the $\alpha v\beta3$ integrin over-expressed in the neovasculature, which is abundant in the glioma margin. The increased local concentration of the nanoagonist activates endothelial $A_{2A}R$ and then specifically up-regulates peri-tumoral BBB permeability. A higher T/B ratio of nanoagonist than that of Den-Reg and Den-PEG in fluorescence imaging verifies the targeting specificity of the nanoagonist.

DCE-MRI has been applied to non-invasively evaluate BBB permeability alterations, in which MR signal changes, as a result of contrast agent leakage into the extracellular extravascular space, could be dynamically monitored [25, 26]. The time-slot for chemotherapeutic injection was optimized at 45 min post nanoagonist administration when the average K_{trans} value was high in the glioma margin but low in surrounding normal brain tissues. The benefit of this image-guided drug delivery strategy was confirmed by timing PTX administration post nanoagonist-mediated BBB opening. The combined treatment not only remarkably increased the therapeutic response of PTX, achieving a longer survival than TMZ, the first-line chemotherapeutic treatment for gliomas, but also prevented the cytotoxic effect of PTX to normal brain tissue. Estimation of the arterial input function (AIF) is the key to accurately determining BBB permeability via DCE-MRI. Direct measurement of AIF from large vessels by blindly estimating the tissue concentration time curves (CTCs) is a mainstream approach. Although the MRI signal from the large vessels is less susceptible to partial volume effect, it indeed succumbs to the T2* effect of the contrast agent, leading to artificial concentration calculations. Additionally, the actual AIF differs from CTC of large vessels due to dispersion of the contrast agent during transportation from the aorta to tissues or from tissues to the veins. The problem is more severe because of the vascular tortuosity in the tumor. In this work, we used a multiple reference tissue method that could estimate the specific AIF for a group of voxels with no constraints on mathematical modeling of AIF but only its smoothness. In this way, the fitting errors of CTCs could be minimized, and a more accurate calculation of dynamic parameters could be achieved.

Conclusion

This work shows the existence of intact tight junctions in the margins of both LGG and HGG from patients. Therefore, a drug delivery strategy to increase BBB permeability in the glioma margin is required to improve therapeutic efficiency and attenuate tumor recurrence rate. With assistance of a nanoagonist specifically tuning TJ integrity in the glioma margins and DCE-MRI dynamically monitoring BBB permeability, it is possible to amplify the efficacy of chemotherapeutics but minimize the side-effects induced by non-specific BBB leakage in normal brain tissue. Overall, nanoagonist-mediated BBB permeability enhancement followed by image-guided drug injection holds promise to improve the response of multiple therapeutics to glioma and minimize their side effects.

Methods

Experimental overview

All animal experiments were approved by the Fudan University Institutional Laboratory Animal Care and Use Committee and performed in accordance with the National Institutes of Health Guidelines for the Care and Use of Laboratory Animals.

Patients

The Huashan Hospital Institutional Review Board approved the protocol, and written informed

consent was obtained from all patients. Human specimens were acquired from patients who underwent craniotomy at the Department of Neurosurgery, Huashan Hospital between 2008 and 2017. Tumor tissues were from three patients with LGG and five patients with HGG. Control brain tissues were from HGG patients who underwent extended resection, including the inferior temporal gyrus and frontal pole. In total, there were 6 male (mean age: 49 years, age range: 29−66 years) and 5 female (mean age: 48 years, age range: 30−68 years) patients. **Figure S1** demonstrates the representative H&E-stained images of LGG, HGG and control brain tissue sections.

Immunofluorescence microscopy imaging studies

Tissues were sectioned with a thickness of 10 µm, fixed with 4% paraformaldehyde (PFA), permeabilized with 0.3% Triton X-100 and blocked with 1% bovine serum albumin (BSA). The slices were incubated with rabbit anti-human ZO-1, $A_{2A}R$ or β3 integrin primary antibody at 4 °C overnight. After washing, the slices were then incubated with mouse anti-human CD31 primary antibody for 24 h. The sections were treated with Alexa-Fluo488 labeled goat anti-rabbit secondary antibody followed by Alexa-Fluo555 labelled goat anti-mouse secondary antibody at room temperature for 2 h and subsequent nuclear staining by 4',6-diamidino-2-phenylindole (DAPI).

In vivo optical imaging studies

Fluorescence images were acquired using an IVIS Spectrum In Vivo Imaging System (Caliper Life Science, Hopkinton, USA). Nine mice bearing orthotropic glioma xenografts were randomly divided into three groups (three mice in each group): Den-PEG, Den-Reg and Den-RGD-Reg. NIR fluorescence images were collected after intravenous (i.v.) administration of the nanoparticles (39.3 mg/kg, excitation filter: 745 nm, emission filter: 800–840 nm) into mouse models bearing the orthotopic human glioma U87MG xenograft. The mice were perfused with saline followed by 4% PFA. The brains were carefully excised and their fluorescence images were captured. The fluorescence intensities were quantified using Living Image 4.0 software (Caliper Life Sciences, Hopkinton, USA).

In vivo MRI studies

In vivo MR imaging was conducted using a 7.0 T micro-MR scanner (Bruker BioSpec, Ettlingen, Germany). The respiration rate was controlled at 30–40 breaths/min. The mice were first anaesthetized with 1–2% isoflurane in 20% oxygen. Nanoagonist

(39.3 mg/kg) or PBS were injected via i.v. injection. Pre-contrast images were acquired as follows: T2-weighted (T2W) images (repetition time (TR)/echo time (TE) = 3800/95 ms; acquisition matrix = 256 × 256; NEX = 4; field of view = 20 × 20 mm; number of slices = 12; slice thickness = 1 mm, rare factor = 8, flip angle = 150°); T1-weighted (T1W) images (TR/TE = 600/11 ms; acquisition matrix = 256 × 256; NEX = 2; field of view = 20 × 20 mm; number of slices = 12; slice thickness = 1 mm, flip angle = 80°). DCE-MRI was obtained using a FLASH axial T1 map (TR/TE = 16/2.8 ms; acquisition matrix = 128× 128; NEX = 1; field of view = 20 × 20 mm; number of slices = 2; slice thickness = 1 mm) with multiple flip angles (5°, 10°, 15°, 20°, 25° and 30°) and T1W imaging (same parameters as FLASH T1 map with flip angles of 25°). At 10 s after DCE-MRI acquisition, Gd^{3+}-DTPA with a dose of 27.4 mg/kg was administered via i.v. injection. The DCE-MRI data were processed by in-house MATLAB (Mathworks, Natick, USA) programs. The Tofts model [27] was used to calculate DCE-MRI kinetic parameters

$$C_t(t) = K_{trans} \int C_p(\tau) \exp\left[-K_{trans}(t\text{-}\tau)/v_e\right] d\tau + v_p C_p(t)] \quad (1)$$

where $C_t(t)$ is the concentration of the contrast agent (CA) in tissue, $C_p(t)$ is the CA concentration in the blood plasma, also known as the arterial input function (AIF), v_e and v_p are the fractional volumes of the extravascular extracelluar space (EES) and plasma respectively, and K_{trans} is the CA transfer rate between the blood plasma and EES. The CA concentration curves were calculated by

$$C_t(t) = (R_1(t) - R_{10})/r_1 \quad (2)$$

where $R_1(t)$ is the longitudinal relaxation rate constant and r_1 is one. The AIFs of glioma and its contralateral tissue were separately estimated by using the multiple reference tissue method [28]. The two AIFs were then rescaled so that their area-under-the-curve were the same and the v_p of normal brain tissue was 4.0 mL/100 mL. The tissue concentration curves and AIFs were then fit to equation (1) using the *lsqcurvefit* function in MATLAB to obtain K_{trans}, v_p, and v_e. Glioma region and its contralateral region were firstly manually drawn for AIF calculation. Then, voxels where v_p is greater than 5.0 mL/100 mL were defined as the glioma parenchyma. The band of 3-voxel (around 0.47 mm) width that surrounds the glioma parenchyma was defined as the glioma margin.

In vivo SPECT/CT imaging

SPECT/CT imaging was performed using a Nano SPECT/CT Plus imager (Bioscan Inc., Washington, USA). Twelve mice bearing orthotropic glioma xenografts were randomly divided into three

groups (four mice in each group). SPECT measurements were performed with ^{99m}Tc-DTPA and the three different groups were treated with Den-PEG, Den-Reg and Den-RGD-Reg, respectively. The mouse models were injected with ^{99m}Tc-DTPA (3.7×10^7 Bq) via i.v. injection alone or 45 min post injection (PI) of the selected nanoparticle. A total of 24 projections were acquired with a minimum of 40,000 counts per projection. Prior to each SPECT imaging, cone-beam CT (180 projections, 55 kVp, 147 µA) images were acquired.

Autoradiography studies

Following SPECT/CT imaging, the mouse brains were carefully isolated, fixed and sectioned with a thickness of 1.0 mm. Next, the brain sections were placed on a phosphor storage screen film (Perkin Elmer, Norwalk, USA) for 15 min. Reading the screens using a Cyclone Pulse Storage Phosphor system (Perkin Elmer, Norwalk, USA) produced autoradiography images that were further analyzed by Optiquant software.

Survival studies

Twenty-eight mice bearing orthotropic glioma xenograft were randomly divided into four groups (seven mice in each group) including PBS, TMZ, PTX, and nanoagonist plus PTX. Both the nanoagonist and the PTX were injected intravenously via tail vein. Paclitaxel (5.0 mg/kg every three days, i.v. injection) was injected at 45 min post administration of nanoagonist (39.3 mg/kg, i.v. injection) in mice bearing glioma xenografts. In control experiments, mice were administrated PTX alone (5.0 mg/kg every three days) or TMZ alone (20 mg/kg daily, oral administration) according to the clinical protocol. The drugs were injected from 7 days after tumor implantation. T2W-MR images of the mouse brain area were collected every 7 days up to 28 days. The total glioma volume was calculated by summing the tumor region in T2W-MRI slides with a thickness of 1.0 mm. Survival of mice was assessed using the Kaplan–Meier method.

Statistical analysis

Quantitative data are provided as medians or means with standard deviation. The Mann-Whitney U test was used to evaluate the difference between two groups. In all cases, a *P* value less than 0.05 indicated statistical significance. Analysis in this study were performed using origin 8.0 software (Microcal Software Inc., Northampton, USA) as well as SPSS 19.0 software (SPSS Inc., Chicago, USA).

Abbreviations

A_{2A}R: adenosine 2A receptor; ASF: actin stress fibre; BBB: blood brain barrier; BBBD: blood brain barrier disruption; c(RGDyK): cyclo(arginine-glycine-aspartic-D-tyrosine-lysine); DCE-MRI: dynamic contrast-enhanced magnetic resonance imaging; Den: dendrimer; GPCRs: G-protein coupled receptor; HGG: high-grade glioma; i.v.: intravenous; LGG: low-grade glioma; MB-FUS: Microbubble-enhanced focused ultrasound; MLC: myosin light chain; MLCP: MLC phosphatase; MR: magnetic resonance; NIR: near-infrared; NVU: neurovascular unit; PAMAM: poly(amidoamine); PEG: polyethylene glycol; PFA: paraformaldehyde; PI: post injection; pMLC: phosphorylated MLC; ROCK: Rho-associated protein kinase; SPECT/CT: single photon emission computed tomography/computed tomography; T/B: target to background; TE: echo time; TJs: tight junctions; TR: repetition time; TUNEL: Terminal-deoxynucleotidyl-transferase mediated dUTP nick end labelling.

Supplementary Material

Materials, methods of confocal fluorescence microscopic imaging, synthesis, characterization, actin stress fibre staining, western blot studies, animal model and histological H&E staining, supplementary figures on synthesis and characterization of nanoagonist, targeting specificity of nanoagonist, H&E stainning images of brain and glioma tissue from patients, K_{trans} values in glioma parenchyma and glioma margin, ZO-1 expression in glioma xenograft margin, TUNEL stained images of glioma xenograft margin. http://www.thno.org/v08p3126s1.pdf

Acknowledgements

Competing Interests

The authors have declared that no competing interest exists.

References

1. Omuro A, DeAngelis LM. Glioblastoma and other malignant gliomas: A clinical review. JAMA. 2013; 310: 1842-50.
2. Wen PY, Kesari S. Malignant Gliomas in Adults. N Engl J Med. 2008; 359: 492-507.
3. Group GM-aTG. Chemotherapy in adult high-grade glioma: a systematic review and meta-analysis of individual patient data from 12 randomised trials. The Lancet. 2002; 359: 1011-8.
4. Van Tellingen O, Yetkin-Arik B, De Gooijer M, Wesseling P, Wurdinger T, De Vries H. Overcoming the blood–brain tumor barrier for effective glioblastoma treatment. Drug Resist Update. 2015; 19: 1-12.
5. Gao X, Li C. Nanoprobes Visualizing Gliomas by Crossing the Blood Brain Tumor Barrier. Small. 2014; 10: 426-40.
6. Juillerat-Jeanneret L. The targeted delivery of cancer drugs across the blood–brain barrier: chemical modifications of drugs or drug-nanoparticles? Drug Discov Today. 2008; 13: 1099-106.
7. Petrecca K, Guiot M-C, Panet-Raymond V, Souhami L. Failure pattern following complete resection plus radiotherapy and temozolomide is at the resection margin in patients with glioblastoma. J Neurooncol. 2013; 111: 19-23.
8. Tali Siegal, Rina Rubinstein, Felix Bokstein, Allan Schwartz, Alexander Lossos, Edna Shalom, et al. In vivo assessment of the window of barrier opening after osmotic blood—brain barrier disruption in humans. J Neurosurg. 2000; 92: 599-605.
9. Marchi N, Angelov L, Masaryk T, Fazio V, Granata T, Hernandez N, et al. Seizure-Promoting Effect of Blood–Brain Barrier Disruption. Epilepsia. 2007; 48: 732-42.
10. Fan C-H, Liu H-L, Ting C-Y, Lee Y-H, Huang C-Y, Ma Y-J, et al. Submicron-bubble-enhanced focused ultrasound for blood–brain barrier disruption and improved CNS drug delivery. PloS one. 2014; 9: e96327.
11. Chopra R, Vykhodtseva N, Hynynen K. Influence of exposure time and pressure amplitude on blood− brain-barrier opening using transcranial ultrasound exposures. ACS Chem Neurosci. 2010; 1: 391-8.
12. Carman AJ, Mills JH, Krenz A, Kim D-G, Bynoe MS. Adenosine receptor signaling modulates permeability of the blood–brain barrier. J Neurosci. 2011; 31: 13272-80.
13. Gao X, Qian J, Zheng S, Changyi Y, Zhang J, Ju S, et al. Overcoming the blood–brain barrier for delivering drugs into the brain by using adenosine receptor nanoagonist. ACS nano. 2014; 8: 3678-89.
14. Gao X, Wang Y-C, Liu Y, Yue Q, Liu Z, Ke M, et al. Nanoagonist-mediated endothelial tight junction opening: A strategy for safely increasing brain drug delivery in mice. J Cereb Blood Flow Metab. 2017; 37: 1410-24.
15. Zheng S, Bai Y-Y, Liu Y, Gao X, Li Y, Changyi Y, et al. Salvaging brain ischemia by increasing neuroprotectant uptake via nanoagonist mediated blood brain barrier permeability enhancement. Biomaterials. 2015; 66: 9-20.
16. Jin Q, Cai Y, Li S, Liu H, Zhou X, Lu C, et al. Edaravone-Encapsulated Agonistic Micelles Rescue Ischemic Brain Tissue by Tuning Blood-Brain Barrier Permeability. Theranostics. 2017; 7: 884.
17. Neuwelt EA, Frenkel EP, D'Agostino AN, Carney DN, Minna JD, Barnett PA, et al. Growth of human lung tumor in the brain of the nude rat as a model to evaluate antitumor agent delivery across the blood-brain barrier. Cancer Res. 1985; 45: 2827-33.
18. Watkins S, Robel S, Kimbrough IF, Robert SM, Ellis-Davies G, Sontheimer H. Disruption of astrocyte–vascular coupling and the blood–brain barrier by invading glioma cells. Nat Commun. 2014; 5: 4196.
19. Kinoshita M, McDannold N, Jolesz FA, Hynynen K. Noninvasive localized delivery of Herceptin to the mouse brain by MRI-guided focused ultrasound-induced blood–brain barrier disruption. Proc Natl Acad Sci U S A. 2006; 103: 11719-23.
20. Aburima A, Wraith KS, Raslan Z, Law R, Magwenzi S, Naseem KM. cAMP signaling regulates platelet myosin light chain (MLC) phosphorylation and shape change through targeting the RhoA-Rho kinase-MLC phosphatase signaling pathway. Blood. 2013; 122: 3533-45.
21. Knipe RS, Tager AM, Liao JK. The Rho kinases: critical mediators of multiple profibrotic processes and rational targets for new therapies for pulmonary fibrosis. Pharmacol Rev. 2015; 67: 103-17.
22. Kim Y, Hechler B, Klutz AM, Gachet C, Jacobson KA. Toward multivalent signaling across G protein-coupled receptors from poly (amidoamine) dendrimers. Bioconjug Chem. 2008; 19: 406-11.
23. de Lera Ruiz M, Lim Y-H, Zheng J. Adenosine A2A receptor as a drug discovery target. J Med Chem. 2013; 57: 3623-50.
24. Jeong JM, Hong MK, Chang YS, Lee Y-S, Kim YJ, Cheon GJ, et al. Preparation of a promising angiogenesis PET imaging agent: 68Ga-labeled c (RGDyK)–isothiocyanatobenzyl-1, 4, 7-triazacyclononane-1, 4, 7-triacetic acid and feasibility studies in mice. J Nucl Med. 2008; 49: 830-6.
25. Blanchette M, Tremblay L, Lepage M, Fortin D. Impact of drug size on brain tumor and brain parenchyma delivery after a blood–brain barrier disruption. J Cereb Blood Flow Metab. 2014; 34: 820-6.
26. Montagne A, Barnes SR, Sweeney MD, Halliday MR, Sagare AP, Zhao Z, et al. Blood-brain barrier breakdown in the aging human hippocampus. Neuron. 2015; 85: 296-302.
27. Tofts PS, Brix G, Buckley DL, Evelhoch JL, Henderson E, Knopp MV, et al. Estimating kinetic parameters from dynamic contrast-enhanced T 1-weighted MRI of a diffusable tracer: standardized quantities and symbols. J Magn Reson Imaging. 1999; 10: 223-32.
28. Yang C, Karczmar GS, Medved M, Stadler WM. Multiple reference tissue method for contrast agent arterial input function estimation. Magn Reson Med. 2007; 58: 1266-75.